NMDA-Like Receptors in the Nervous System of the Crab *Neohelice granulata*: A Neuroanatomical Description

Yanil Hepp, Martín Carbó Tano, María Eugenia Pedreira, and Ramiro A.M. Freudenthal*

Laboratorio de Neurobiología de la Memoria, Facultad de Ciencias Exactas y Naturales, dep. Fisiología y Biología Molecular y Celular, Universidad de Buenos Aires, Ciudad Universitaria, Ciudad Autónoma de Buenos Aires, Argentina.

ABSTRACT

N-Methyl-D-aspartate receptors (NMDARs) are involved in learning and memory processes in vertebrates and invertebrates. In *Neohelice granulata*, NMDARs are involved in the storage of associative memories (see references in text). The aim of this work was to characterize this type of glutamate receptor in *Neohelice* and to describe its distribution in the central nervous system (CNS). As a first step, a detailed study of the CNS of *N. granulata* was performed at the neuropil level, with special focus on one of the main structures involved in this type of memory, the supraesophageal ganglion, called central brain. The characterization of the NMDAR was achieved by identifying the essential subunit of these receptors, the NR1-like subunit. The NR1-like signals were found via western blot and immunohistochemistry techniques in each of the major ganglia: the eyestalk ganglia, the central brain, and the thoracic ganglion. Western blots yielded two bands for the crab NR1-like subunit, at ~88 and ~84 kDa. This subunit is present in all the major ganglia, and shows a strong localization in synaptosomal membranes. NMDARs are distributed throughout the majority of each ganglion but show prominent signal intensity in some distinguishable neuropils and neurons. This is the first general description of the *N. granulata* nervous system as a whole and the first study of NMDARs in the CNS of decapods. The preferential localization of the receptor in some neuropils and neurons indicates the presence of possible new targets for memory processing and storage. J. Comp. Neurol. 521:2279–2297, 2013.

INDEXING TERMS: invertebrate; decapod; ganglion; neuropil; NR1 subunit; Neohelice granulata

N-Methyl-D-aspartate receptors (NMDARs) are one of the three pharmacologically distinct subtypes of glutamatergic ionotropic receptors, and they are present at many of the pre- and postsynapses of the central nervous system (CNS) (reviewed in Van Dongen, 2009). These receptors form heteromeric complexes, which are usually comprised of essential NR1 subunits and distinct NR2 (A, B, C, and D) or NR3 subunits (Dingledine et al., 1999; Hollmann, 1999; Cull-Candy et al., 2001). The NR1 subunit possesses an affinity for glycine, which modulates the activation of the receptor upon binding to other subunits (Furukawa and Grouaux, 2003; Papadakis et al., 2004). The opening of NMDAR channels, which are permeable to calcium and sodium, requires simultaneous glutamate binding and postsynaptic membrane depolarization (Mayer et al., 1994; McBain and Mayer, 1994; Dingledine et al., 1999). The remarkable molecular property of the voltage-dependent blockade of glutamate-induced calcium flux suggests that NMDARs would serve as the "Hebbian coincidence detectors" which underlie associative learning (Sweatt, 2003). In addition, cellular studies have suggested that NMDARs are implicated in triggering the long-term potentiation and long-term depression of synaptic transmission, which are neuromodulatory processes important for learning and memory (Cain, 1997; Carew, 2000).

Grant sponsor: University of Buenos Aires; Grant number: UBACYT X618; Grant sponsor: FONCYT-ANPCYT; Grant numbers: PICT 2010-0391; PICT 2006-01161 and PICT 2008-02056

The last two authors contributed equally to this work.

*CORRESPONDENCE TO: Ramiro A.M. Freudenthal, Laboratorio de Neurobiología de la Memoria, Facultad de Ciencias Exactas y Naturales, dep. Fisiología y Biología Molecular y Celular, Universidad de Buenos Aires, IFIBYNE-Conicet. 2 piso, pab. II, Ciudad Universitaria, Ciudad Autónoma de Buenos Aires, CP: 1428, Argentina. E-mail: rfreudenthal@yahoo.com or ramirof@fbmc.fcen.uba.ar.

Received July 30, 2012; Revised November 30, 2012; Accepted December 11, 2012

DOI 10.1002/cne.23285

Published online December 14, 2012 in Wiley Online Library (wileyonlinelibrary.com)

A considerable amount of evidence from different studies, which have used a variety of paradigms and tasks, supports the relevant role of NMDARs in diverse behavioral outcomes (Morris et al., 1986; Tan et al., 1989; Miserendino et al., 1990; Richard et al., 1994; Weldon et al., 1997; Gutiérrez et al., 1999). Most of this extensive research has been restricted to vertebrate species. Nevertheless, several studies in invertebrates have demonstrated that glutamate is a neurotransmitter at the neuromuscular junction and in the CNS (Bicker et al., 1988; Sinakevitch et al., 2001; Strausfeld, 2002). In addition, several homologs to mammalian glutamate receptors have been identified in invertebrates. The first description of NMDA-like receptors was in the visual interneurons of crayfish (*Cherax destructor*) by Pfeiffer-Linn and Glantz (1991), using an electrophysiological approach. After that important study, diverse reports identified the presence of NMDA-like receptors in decapods using pharmacological and electrophysiological techniques (Parnas et al., 1994, 1996; Burgess and Derby, 1997; Schramm and Dudel, 1997). Employing immunohistochemical techniques, NMDA-like receptors were reported in the neuromuscular junctions of two crustaceans, crayfish (Feinstein et al., 1998) and the cyprid *Balanus amphitrite* (Gallus et al., 2010). Additionally, several studies in other invertebrate models have also reported the presence of NMDA-like receptors. Evidence has also demonstrated their existence in mollusks, such as diverse bivalves (Todoroki et al., 1999; Shibata el al., 2001), the freshwater gastropod *Lymnaea stagnalis* (Moroz et al., 1993) and the sea slug *Aplysia californica* (Dale and Kandel, 1993; Ha et al., 2006). Molecular evidence of the presence of NMDA-like subunits has been found in annelids, nematodes, and insects (Ultsch el at., 1993; Chiang et al., 2001, 2002; Brockie et al., 2001; Xia et al., 2005; Zannat et al., 2006; Grey et al., 2009; Bonasio et al., 2010).

Regarding the role of NMDARs in invertebrate models, NMDAR-dependent long-term potentiation was reported in *Aplysia californica* (Lin and Glanzman, 1994, 1997; Roberts and Glanzman, 2003), and their role in learning and memory processes was demonstrated in several other species (*Lymnaea stagnalis*: Browing and Lukowiak, 2008; Rosenegger and Lukowiak, 2010; *Apis mellifera*: Si et al., 2004; Müβig et al., 2010; *Drosophila melanogaster*: Xia et al., 2005; Wu et al., 2007; *Caenorhabditis elegans*: Kano et al., 2008; Amano and Maruyama, 2011).

Intense research performed in the crab *Neohelice granulata* (formerly *Chasmagnathus granulatus*) has indicated that NMDA-like receptors are involved in long-term memory (LTM), playing an important role in memory consolidation and reconsolidation (Pedreira et al., 2002; Troncoso and Maldonado, 2002). The systemic administration of the vertebrate NMDAR antagonists MK-801 and AP5 disrupts both consolidation and reconsolidation processes of an associative memory paradigm, which has been widely studied in our laboratory (Maldonado, 2002; Pedreira and Maldonado, 2003; Frenkel et al., 2005; Romano et al., 2006; Federman et al., 2009; Pérez-Cuesta and Maldonado 2009; Hepp et al., 2010). The function of these receptors is also necessary for the acquisition of extinction memory but not for its consolidation (Pérez-Cuesta et al., 2007). These pharmacological-behavioral experiments were the initial evidence that suggested the existence of NMDA-like receptors in crabs.

Considering both the relevance of NMDARs in mnesic processes and the shortage of CNS descriptions in decapods, the goals of the present article are to describe the major ganglia of the *N. granulata* nervous system, to characterize the NR1-like subunit, and to study the distribution of NMDA-like receptors in the crab CNS. To date, the available neuroanatomical descriptions of *N. granulata* are based on the pioneering studies by Sandeman (Sandeman, 1982; Sandeman et al., 1992), and on a general description of the *Neohelice* CNS as reported by Bond-Buckup et al. (1991). Thus, to better understand the localization of NMDA-like receptors, we first described the CNS of *N. granulata* at the neuropil level, including the eyestalk ganglia (EG), the central brain (CBr), and the thoracic ganglion (TG). The CBr processes sensory inputs, integrates multimodal

Abbreviations

AMPN	Anterior medial protocerebral neuropil
AnN	Antenna II neuropil
A_INv	Antenna I nerve
A_{II}Nv	Antenna II nerve
CA	Cerebral artery
CB	Central body
CBr	Central brain
CC	Circumesophageal connectives
CG	Commissural ganglion
CNS	Central nervous system
EG	Eyestalk ganglia
HB	Hemiellipsoid body
NR1-ir	NR1-like immunoreactivity
La	Lamina
LAN	Lateral antenna I neuropil
Lo	Lobula
LPc	Lateral protocerebrum
LTM	Long-term memory
MAN	Median antenna I neuropil
Me	Medulla
MT	Medulla terminalis
MPc	Median protocerebrum
NR1-ir	NR1-like immunoreactivity
OGT	Olfactory globular tract
O	Esophagus
OL	Olfactory lobes
OMNv	Oculomotor nerve
PB	Protocerebral bridge
PMPN	Posterior medial protocerebral neuropil
PI	Propidium iodide
PT	Protocerebral tract
SA	Sternal artery
TN	Tegumentary neuropil
TNv	Tegumentary nerve
TG	Thoracic ganglion

information, and has been shown to be extremely important for learning and memory formation (Freudenthal et al., 1998; Romano et al., 2006; Merlo and Romano, 2007, 2008; Federman et al., 2009, 2012; Fustiñana et al., 2010; and see Tomsic et al., 2003). The consolidation of this associative learning (Maldonado, 2002) is modulated by angiotensin II (Frenkel et al., 2005, 2010) and is dependent on the activation of several kinases: cAMP-dependent protein kinase (PKA) and mitogen-activated protein kinase (MAPK) (Locatelli and Romano, 2005; Feld et al., 2005). The transcriptional events that take place during consolidation are regulated by a transcription factor of the Rel/NF-kappaB family (Freudenthal et al., 1998; Freudenthal and Romano, 2000). Taken together, these molecular studies suggest that the CBr rather than the TG is the neuronal substrate where this LTM consolidation occurs. Therefore, the brain is the primary target of our description. The goals of this report were to obtain a neuroanatomical description of *N. granulata* CNS, and to identify the areas of abundant NMDA-like receptors. The exact localization of NMDA-like immunoreactivity will be indispensable to understand NMDA-dependent LTM processing and storage in *N. granulata*.

Abbreviations

AMPN	Anterior medial protocerebral neuropil
AnN	Antenna II neuropil
A_INv	Antenna I nerve
A_{II}Nv	Antenna II nerve
CA	Cerebral artery
CB	Central body
CBr	Central brain
CC	Circumesophageal connectives
CG	Commissural ganglion
CNS	Central nervous system
EG	Eyestalk ganglia
HB	Hemiellipsoid body
NR1-ir	NR1-like immunoreactivity
La	Lamina
LAN	Lateral antenna I neuropil
Lo	Lobula
LPc	Lateral protocerebrum
LTM	Long-term memory
MAN	Median antenna I neuropil
Me	Medulla
MT	Medulla terminalis
MPc	Median protocerebrum
NR1-ir	NR1-like immunoreactivity
OGT	Olfactory globular tract
O	Esophagus
OL	Olfactory lobes
OMNv	Oculomotor nerve
PB	Protocerebral bridge
PMPN	Posterior medial protocerebral neuropil
PI	Propidium iodide
PT	Protocerebral tract
SA	Sternal artery
TN	Tegumentary neuropil
TNv	Tegumentary nerve
TG	Thoracic ganglion

MATERIALS AND METHODS

Animals

We used adult male intertidal crabs (*Neohelice granulata*, formerly *Chasmagnathus granulatus*), measuring 2.7–3.0 cm across the carapace and weighing ~17.0 g. The crabs were collected from water <1 m deep in narrow coastal inlets (*rías*) of San Clemente del Tuyú, Buenos Aires Province, Argentina. Once transported to the laboratory, they were housed in plastic tanks (35 × 48 × 27 cm) filled to a depth of 2 cm with diluted marine water (Red sea fish pharm, Eilat, Israel) with a salinity of 1.0–1.4% and a pH of 7.4–7.6. The water was changed every 2 days. The holding room was maintained on a 12-hour light–dark cycle (lights on from 07:00–19:00 h) and the temperature was maintained between 22–24°C. The reported research was conducted in accordance with the local regulations for the care and use of laboratory animals. All efforts were made to minimize animal suffering and the number of animals used.

CNS low-magnification drawings

CNS scheme

The animals were anesthetized by immersion in an ice/salt-water mix for 5 minutes. Dissections of the CNS were made, including the three major interconnected ganglia. The fresh tissue was immersed in crab saline solution and visualized with a microscope (Infinity 2, Olympus CX31). The drawings were made at 40× magnification using a camera lucida attachment to the microscope.

CBr maps

Crab CBr were dissected as described previously and fixed in 4% paraformaldehyde (PFA) in 0.1 M phosphate-buffered saline (PBS) ph 6.8, at room temperature for 2 hours with constant agitation. After four buffer washes (15 minutes each, at room temperature), the ganglia were incubated for 10 minutes in a solution of propidium iodide (PI, 1.5 mM, without RNase), used as a cellular counterstain, and washed again with PBS-0.3% Tween 20 (PBS-T) as described previously. Finally, the tissues were dehydrated and mounted in methyl salicylate (Sigma, St. Louis, MO). The PI treatment without RNase stains nuclei and RNA-rich cytoplasm, outlying neuropils (Rieger et al., 2010).

Synaptosomal membrane protein extracts

The animals were anaesthetized by immersion in an ice/salt-water mix for 5 minutes. The EG, CBr, and TG were then dissected. For each sample, 20 EG, 20 CBr, and 20 TG were pooled in 1 ml of buffered crab saline solution (pH 7.4). The extracts enriched in synaptosomal membranes were obtained as follows: The dissected

tissues were homogenized in 750 μl of cold homogenization buffer (20 mM Tris-HCl, 900 mM sucrose, 1 mM EDTA, pH 7.8), with protease inhibitors (phenylmethylsulphonyl fluoride [PMSF] 0.5 mM, aprotinin 10 μg/ml, leupeptin 10 μg/ml, pepstatin A 1 μg/ml) with a glass-glass homogenizer. The tissue homogenates were centrifuged (4°C, 1,000*g*, 10 minutes) to produce a pellet (P1) and a supernatant (S1). S1 was collected and the P1 was resuspended in 500 μl of the homogenization buffer and recentrifuged (4°C, 1,000*g*, 10 minutes) to obtain a pellet (P1′) and supernatant (S1′). P1′ was resuspended in 30 μl of cold hyperosmotic buffer (20 mM HEPES, pH 7.9; 1.2 M KCl; 1.5 mM $MgCl_2$; 0.4 mM EDTA; 0.5 mM DTT; 50% glycerol, pepstatin A, 1 μg/ml; leupeptin, 10 μg/ml; 0,5 mM PMSF; and aprotinin, 10 μg/ml) and centrifuged (4°C, 10,000*g*, 15 minutes). The supernatant corresponds to the nuclear extract and the pellet was discarded. S1 and S1′ were combined and centrifuged at 13,000*g* for 30 minutes to obtain a pellet (P2, enriched in synaptosomes) and a supernatant (S2, cytoplasmatic extract). P2 was resuspended in 200 μl of cold hypo-osmotic buffer (5 mM Tris-HCl, 50 mM $CaCl_2$, pH 8.1), sonicated at 49% for 3 sec and centrifuged (15,800*g*, 50 minutes) to produce a pellet (P3, enriched in synaptosomal membranes) and a supernatant (S3, enriched in synaptosomal content). P3 was resuspended in 30 μl of hypo-osmotic buffer-1% sodium dodecyl sulfate (SDS). For only the treatment of synaptosomal membranes with detergents of increasing strength, P3 was resuspended in 30 μl of hypo-osmotic buffer-1% Triton X-100 and was centrifuged to produce a supernatant (S4, synaptosomal membrane Triton X-100) and a pellet (P4). P4 was resuspended in 30 μl of hypo-osmotic buffer-1% SDS (synaptosomal membrane-SDS). The extracts were stored at −80°C until use. The extracts enriched in synaptosomal membranes from mice were obtained using the protocol mentioned above, but the sucrose concentration of the homogenization buffer was 320 mM. All of the procedures were performed with the tissue fractions while maintaining the temperature at 4°C. The protein concentrations in the resultant extracts were determined with a Pierce BCA Protein Assay Kit (Thermo Scientific, Waltham, MA; 23227).

Western blot assays

Loading buffer (4×) was added to each sample (35 μg of protein), which was then denatured (boiled for 5 minutes at 100°C) and immediately placed on ice. Then the samples were electrophoresed using 10% SDS-polyacrylamide gel electrophoresis (PAGE) at 100 V for 1 hour and then electroblotted to PVDF membrane (Bio-Rad, Hercules, CA) at 100 V for 1 hour. The blots were blocked in blocking buffer (10% low-fat dry milk in Tris-buffered saline-0.1% Tween 20 [TBS-T], pH 7.6) for 1 hour at room temperature. After two 15-minute washes with TBS-T, the blots were incubated overnight (4°C) with a primary antibody, rabbit polyclonal anti-rat NMDAR1. For immunoblotting with the AB1516 antibody (Chemicon, Temecula, CA; 0.1 μg/μl), a 1:100 dilution in PBS-T was used. After six 10-minute washes with TBS-T, the blots were incubated with horseradish peroxidase (HRP)-conjugated goat anti-rabbit IgG (1:5,000 dilution in TBS-T, 1 hour, 25°C; Santa Cruz Biotechnology, Santa Cruz, CA; sc-2030), followed by six washes of 10 minutes each with TBS-T. Detection was made with a Luminol chemiluminescence kit (Santa Cruz Biotechnology) as described by the manufacturer, and the signals were digitized by a FUJI FILM-Intelligent Dark Box II apparatus with image reader LAS-1000 software. The protein size was estimated by its relative mobility using ImageJ 1.293 software (NIH, Bethesda, MD) and correlating these measurements with the molecular weights of prestained standard proteins (Full-Range Rainbow Molecular Weight Markers: 12-225 kDa, Amersham, Arlington Heights, IL).

Antibody characterization

Because specific antibodies for crab NMDARs were not available, we used a commercial polyclonal antibody raised against mammalian NMDAR. The AB1516 (Chemicon, Lot no. 200060436) antibody was selected from the commercially available antibodies because it was successfully employed in a decapod crustacean to identify NMDA-like glutamate autoreceptors in the crayfish neuromuscular junction (Feinstein et al., 1998). This antibody was raised in rabbits using a synthetic peptide corresponding to the C-terminus of rat NR1 receptor subunit (amino acids 909–938: LQNQKDTVLPRRAIEREEGQLQLCSRHRES) as the immunogen. This antibody is predicted to recognize all major splice variants (1a, 1b, 2a, and 2b) and does not show crossreactions with other glutamate receptor subunits. Western blot analysis showed that the antibody labels a single band at ~120 kDa in rabbit and rat extracts (Fletcher et al., 2000). In addition, this antibody shows crossreactivity with monkeys, gerbils, felines, and fish, due to high sequence homology. Actin signals were revealed with a rabbit polyclonal IgG antibody (1:5,000 dilution; Santa Cruz Biotechnology; sc-1616-R, Lot no. 1105). This polyclonal antibody against actin was raised against a peptide that maps at the C-terminus (aa 325–375, gi|4501885) of actin of human origin. The antigen peptide is coincident with the *Neohelice* actin (gi|28435512) C-terminus in 21 amino acids. In western blots, this antibody labels a single band of ~42 kDa.

Competition assays

For homologous preadsorption tests the primary antibody (AB1516, 0.1 μg/μl) was preadsorbed (1:1) with a synthetic peptide (aa 909-938, Millipore, Bedford, MA; AG344, 1 μg/μl) overnight at 4°C with constant agitation. For the heterologous preadsorption tests, the protein extract was obtained as follows: crab synaptosomal membrane extracts, prepared as mentioned above, were run on SDS-PAGE (six wells with 50 μg of protein each). After electrophoresis, the gel zone between 76 and 102 kDa was cut and transferred to a 1.5-ml fresh tube with 1 ml of MiliQ sterilized water with protease inhibitors (PMSF, 0.5 mM; aprotinin, 10 μg/ml; leupeptin, 10 μg/ml; pepstatin A, 1 μg/ml). After incubation for 1 hour at room temperature with constant agitation the solution was collected. This process was repeated. Then the gel fractions were transferred to a fresh filter tube and centrifuged at 10,000*g* for 35 minutes. The filtered solution was collected, pooled with previous solutions, and concentrated in a Speed-vac for 2 hours.

Immunohistochemistry techniques

Crab EG, CBr, and TG were dissected as described above and fixed in 4% PFA in 0.1 M PBS at room temperature for 2 hours with constant agitation.

Whole-mount immunohistochemistry

After four buffer washes (15 minutes each at room temperature), the tissues were blocked with 2% bovine serum albumin (BSA, Sigma) in PBS-1% Triton X-100 (PBS-Tx) for 2 hours at room temperature with constant agitation. The primary antirat NMDAR1 antibody (Chemicon, AB1516, rabbit) was used for tissue immunolabeling at a dilution of 1:50 in PBS-1% Tween 20 (PBS-T). After incubation at 4°C for 48 hours with constant agitation, the tissues were washed with several changes of PBS for 2 hours at room temperature. Antibody labeling was visualized by incubating the tissues with an Alexa Fluor 488-labeled goat antirabbit antibody (Invitrogen, La Jolla, CA; A11008) at a dilution of 1:500 at 4°C for 2 hours. The tissues were washed with several changes of PBS-T for 2 hours at room temperature. For cases in which PI was used, the tissues were incubated for 10 minutes in 1.5 mM propidium iodide, washed several times with PBS-T, and finally dehydrated in increasing ethanol concentrations in PBS and coverslipped with methyl salicylate (Sigma).

Tissue section immunohistochemistry

After four buffer washes (15 minutes each, at room temperature), the tissues were immersed in low-melting agarose 7% (Promega, Madison, WI; V-3841) at 45°C. The sections were obtained using a vibratome (Vibratome 1000 classic). The section thickness was 200 μm for CBr and EG, and 300 μm for TG. The sections were blocked with 2% bovine serum albumin (BSA; Sigma) in free-floating PBS-1% Triton X-100 (PBS-Tx) for 2 hours at room temperature with constant agitation. The employed immunolabeling protocol with the primary NMDAR1 antibody (Chemicon; AB1516) was the same as that with the whole-mount tissue.

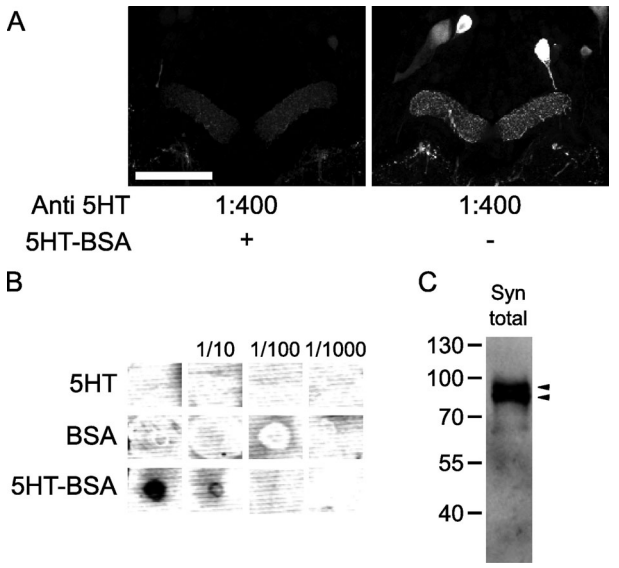

Figure 1. Specificity of serotonin signal and Synapsin western blot. **A**: Preincubation of the serotonin antibody with serotonin crosslinked to BSA reduces the immunochemical signal seen in the central brain. **B**: Dotblot of serotonin, BSA, and serotonin-BSA, showing immunoreactivity only serotonin crosslinked to BSA. **C**: Western blot of total synaptosomal proteins assayed for synapsin (Synorf antibody), yielded two bands of ~90 kDa. Scale bar = 100 μm.

For serotonin immunolabeling, the sections were washed with PBS-0.5% Triton X-100, blocked for 1 hour (2% normal goat serum), and incubated overnight at room temperature with primary antibody (1:400 rabbit anti-5HT; Immunostar, Hudson, WI). The sections were washed again on the following day, blocked, and then incubated overnight at room temperature with Cy3-labeled secondary antibody (1:500 goat antirabbit; Jackson Immunoresearch, West Grove, PA) in PBS-0.5% Triton X-100. Specificity of the serotonin signal was assayed preincubating the primary antibody with serotonin crosslinked to BSA (Fig. 1A). Only serotonin crosslinked to BSA showed immunoreactivity (Fig. 1B).

For double labeling immunochemistry 200-μm sections were blocked with 1% BSA (Sigma) in PB-0.3% Triton X-100 for 1.5 hours at room temperature with constant agitation. The primary antibodies, NMDAR1 antibody (rabbit, Chemicon, AB1516) and anti-synapsin (mouse, 3C11, anti SYNORF1) (Klagges et al., 1996; Frenkel et al., 2012) were used for tissue immunolabeling at a dilution of 1:50 and 1:30, respectively, in PBS-0.3% Tween 20 (48 hours).

Antibody labeling was visualized by incubating the tissues with an Alexa Fluor 488-labeled goat antimouse antibody (Invitrogen; A11001) and tetramethylrhodamine isothiocyanate (TRITC)-labeled antirabbit IgG secondary antibody (ab50598) in PBS-0.3% Tween 20, at a dilution of 1:500 for both antibodies, at 4°C for 3 hours.

Finally, the sections were dehydrated in glycerol-PBS (50:50) for 30 minutes and coverslipped with glycerol-PBS (80:20). When assayed in western blot, the anti-synapsin antibody develops a double band of ~90 kDa (Fig. 1C), similar to the results obtained for *Drosophila* and other crustaceans (Harzsch and Hansson, 2008).

Fluorescence in tissue samples was visualized using a confocal laser-scanning microscope (Olympus FV300, Japan) equipped with a 488-nm argon laser and a 543-nm HeNe Green, a Plan N 4× objective (NA 0.1), a UplanFl 10× objective (NA 0.3), a UplanFl 20× objective (NA 0.5), and a dichroic cube SDM 570 to split the acquisition channels. Ganglia used to sketch NR1-like protein distribution were counterstained with PI or without counterstaining. The PI and the autofluorescence were used as guides to outline neuropils.

The specificity of the secondary antibody was evaluated by carrying out the immunohistochemistry protocol without the primary antibody. This control was performed in the CNS of *Neohelice* and revealed no staining. Black and white immunohistochemistry images from the stacks were background subtracted (rolling ball), kalman filtered, inverted, adjusted for brightness/contrast, and z-projected for the reported number of slices.

The comparative particle analysis of anterior medial protocerebral neuropil and tritocerebral neuropils was carried out in six whole-mount CBr. Confocal stack images (taken every 3 μm in the Z axes) were background subtracted, kalman filtered, and duplicated. The desired areas (anterior medial protocerebral neuropil and tritocerebral neuropils) were defined in the X, Y, and Z axes, one for each copy, and all other pixels were leveled to zero. The NR1-like signal was delimited by threshold (Max Entropy) in each area, overthreshold pixels were taken to maximum (255, in 8-bit images), and the rest were lowered to zero. The maximum diameter (Feret's diameter) was calculated for all the resulting particles. The mean Feret's diameter was calculated for the particles between 2 and 10 μm for each area, and significant differences were estimated by a paired *t*-test. Image processing was performed using ImageJ 1.40g software (http://rsb.info.nih.gov/ij/).

RESULTS

CNS of the crab Neohelice granulata

According to their embryological origin, the crab nervous system is classified traditionally in three main divisions: protocerebrum, deutocerebrum, and tritocerebrum (Nassel and Elofsson, 1987). In decapod crustaceans, the protocerebrum can be subdivided into three parts: optic neuropils, lateral protocerebrum, and median protocerebrum, as indicated by Sandeman et al. (1992). The optic neuropils and lateral protocerebrum (terminal medulla and hemiellipsoid body) are contained in the optic lobes; these structures will be considered together as the EG. The median protocerebrum is part of the CBr, and the rest of the ganglion originates from the deutocerebrum and tritocerebrum. In the majority of brachyurans the thoracic ganglion mass is formed by the fusion of the thoracic and the abdominal ganglia (Sandeman, 1982; McLaughlin, 1983). The nomenclature employed for the general description of ganglia and principal nerves is in accordance with the pioneering works of Bond-Buckup et al. (1991), Sandeman et al. (1992), and Richter et al. (2010).

General description

The central nervous system of the crab is composed mainly of the EG, the CBr, and the TG (Figs. 2A,B, 3, 7). These structures were visualized together with all principal connectives, and a general scheme of the *Neohelice* CNS was drawn (Fig. 2A). Like most malacostracan crustaceans, the lateral protocerebrum and the three optic neuropils are named from the periphery to the center as the lamina (La), medulla (Me), and lobula (Lo), and they are located in the eyestalks (Sztarker et al., 2009) (Figs. 2A,B, 3D, 7A). The EG are linked to the CBr by the protocerebral tract and the oculomotor nerve (Fig. 2A). The CBr is broader than it is long (Figs. 2A, 4), and in animals with a carapace length of 2.7–3.0 cm, its approximate size is ~1.1 mm in length and ~2.4 mm in width. The CBr is located medially in the cephalothorax and contains different neuropils; the most conspicuous are the olfactory lobes, two structures discernible as separate areas composed of glomerular neuropils lying on each side of the brain (Figs. 2A, 4). This ganglion centrally presents a visible hemolymph vessel (cerebral artery) (Fig. 4). Two principal connectives, the circumesophageal connectives, are located posterior to the CBr (Fig. 2A). These connectives surround the esophagus and reach the commissural ganglia (Fig. 2A), which contains somata of heterogeneous size and connections to the stomatogastric system. After the esophagus, the circumesophageal connectives are linked by a small commissure, the postesophageal commissure (Fig. 2A). The circumesophageal connectives end at the anterior part of the TG, located ventrally in the

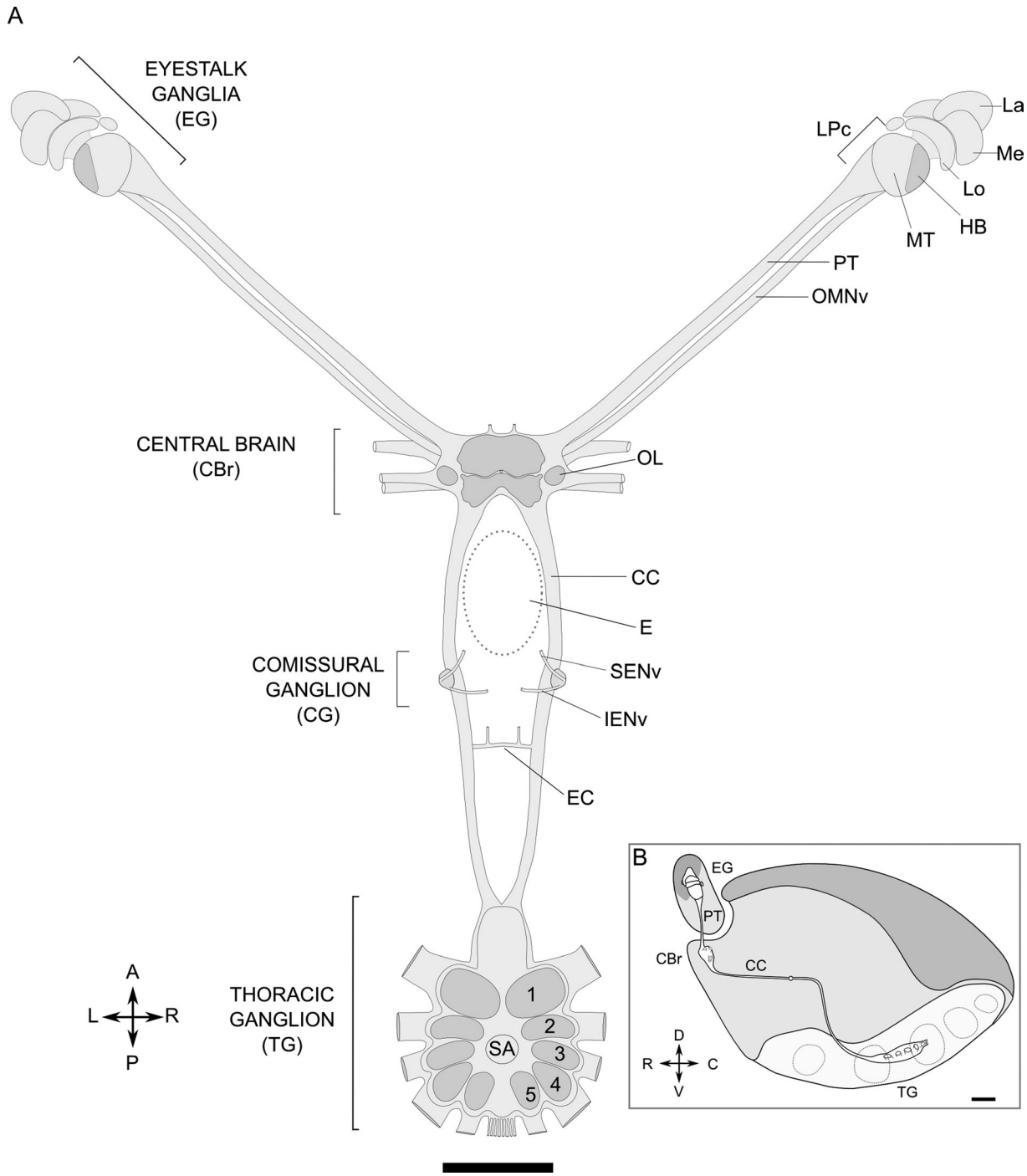

Figure 2. CNS of *Neohelice granulata*. **A**: General scheme. The optic neuropils (lamina, La; medulla, Me; lobula, Lo) and the lateral protocerebrum (LPc) are contained in the eyestalk ganglia (EG). The protocerebral tracts (PT) and the oculomotor nerves (OMNv) project from the EG to the central brain (CBr). In this ganglion, two conspicuous structures, the olfactory lobes (OL), are discernible. The posterior nerves, termed circumesophageal connectives (CC), surround the esophagus (E) and reach the commissural ganglia (CG). The CC are linked by the postesophageal commissure (EC) and end in the thoracic ganglion (TG), where five pairs of symmetrical limb-associated neuropils are identified (from 1 to 5). In the center the sternal artery (SA). The cross indicates positions: A, anterior; P, posterior; L, left and R, right. **B**: Diagram of the crab body containing the central nervous system. Lateral view, excluding the chelae and limbs, showing the EG located in the eyestalks, the CBr situated medially in the anterior ventral side, and the CC running in a rostrocaudal direction to the CG, then directed toward the most ventral surface of the cephalothorax, ending in the TG. The cross indicates positions: D, dorsal; V. ventral; R, rostral and C, caudal. Scale bar = 2 mm.

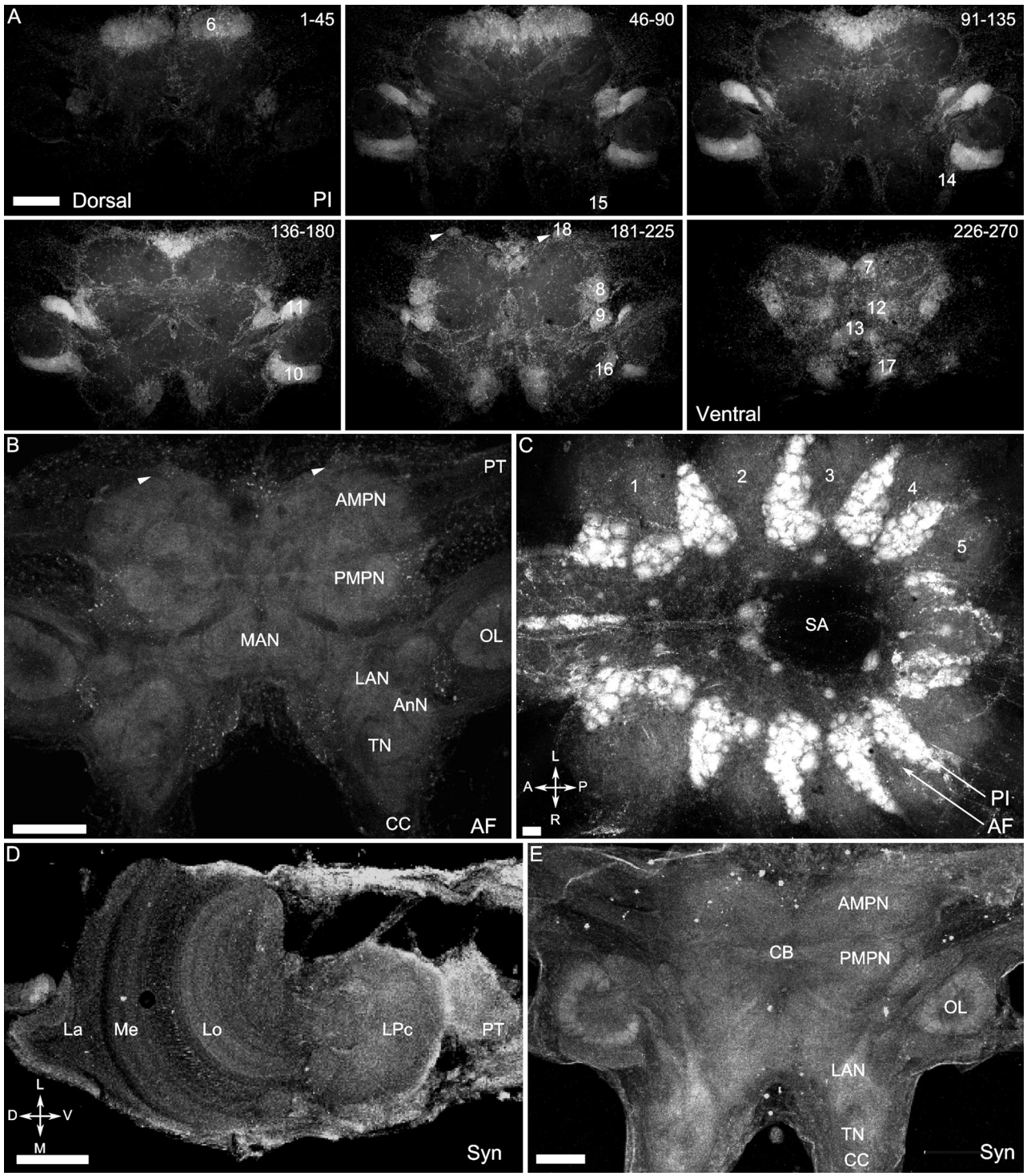

Figure 3. Markers used to study the *Neohelice granulata* nervous system. **A**: Dorsal-ventral scans of PI-stained central brain. Slices of 3 μm thick were taken (1–270 μm) and stacked each 45 μm (15 slices × 6: 1–45; 46–90; 91–135; 136–180; 181–225; 226–270). Numbers indicate different cell clusters identified in each stack. White arrowheads indicate the 18th clusters **B**: Central brain neuropils visualized by autofluorescence (AF). Protocerebral tract (PT); anterior medial protocerebral neuropil (AMPN); posterior medial protocerebral neuropil (PMPN); median antenna I neuropil (MAN); olfatory lobe (OL); lateral antenna I neuropil (LAN); antenna II neuropil (AnN); tegumentary neuropil (TN); circumesophageal connectives (CC). **C**: PI-stained thoracic ganglion (PI). AF, autofluorescence. Abbreviations as in Figure 2. **D,E**: Synapsin-like immunoreactivity (SYN) in the eyestalk ganglia. Abbreviations as in Figure 2 (D), central brain (E). Central body (CB); abbreviations as in Figure 3B. Scale bars = 200 μm.

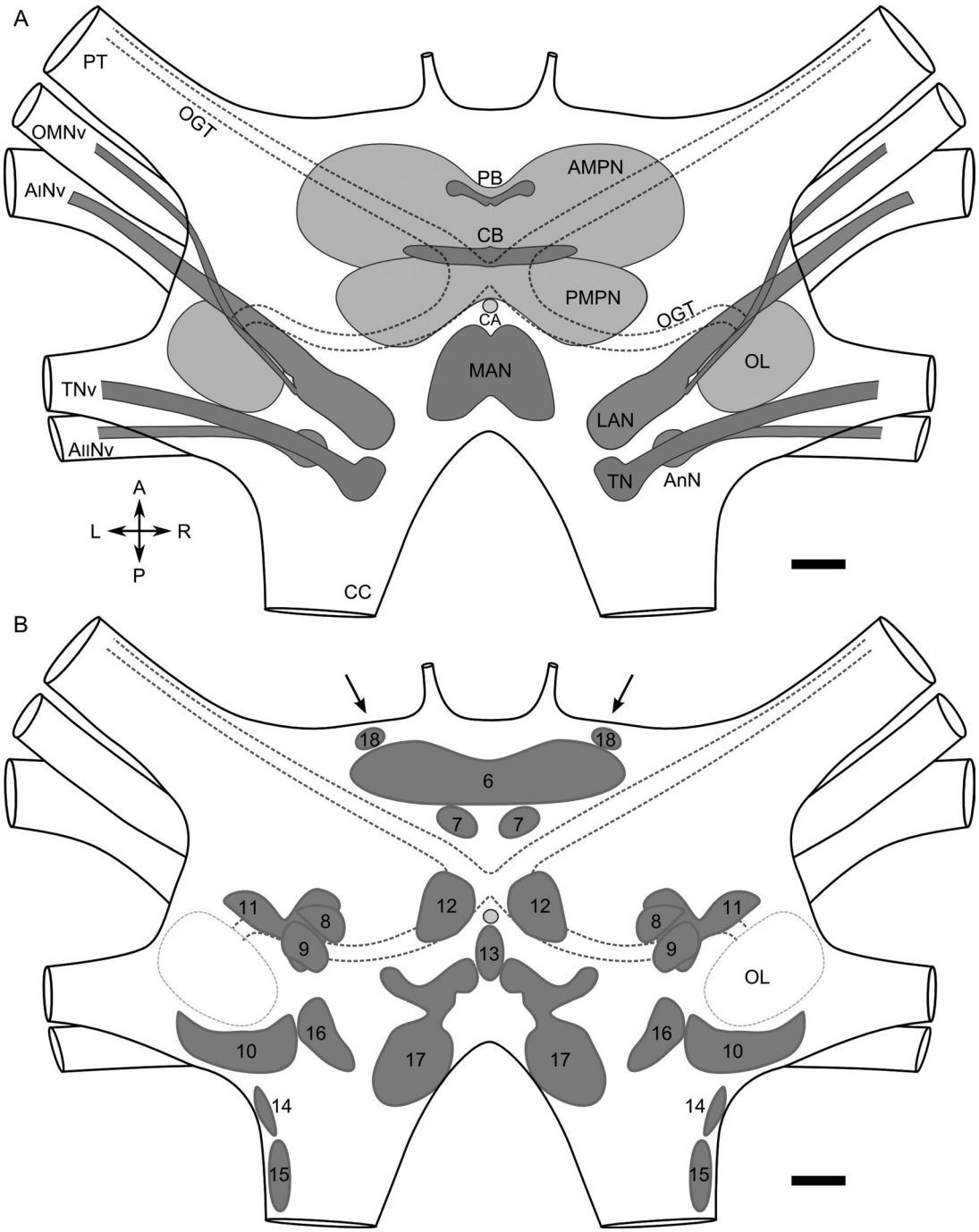

Figure 4. The *Neohelice* central brain. **A**: Map of neuropils. From anterior to posterior: anterior and posterior medial protocerebral neuropils (AMPN and PMPN, respectively); protocerebral bridge (PB); central body (CB); olfactory lobes (OL), which are linked with the lateral protocerebrum in the eyestalk ganglia via the olfactory globular tract (OGT); median antenna I neuropil (MAN); lateral antenna I neuropils (LAN) with their nerves (AINV and OMNv); antenna II neuropils (AnN) with their nerves (AIINv); tegumentary neuropils (TN) with their nerves (TNv). CA, cerebral artery; CC, circumesophageal connectives; OGT, olfactory globular tract (dotted lines). The cross indicates positions: A, anterior; P, posterior; L, left and R, right. **B**: Map of cell clusters. Thirteen groups of cell bodies were recognized, denoted 6th to 17th after Sandeman's description, and the extra pair identified was named the 18th cluster (black arrows). All clusters are symmetrical pairs, except for 6th and 13th. Olfactory lobes (OL) and olfactory globular tract are represented with dotted lines. Scale bars = 200 μm.

cephalothorax (Fig. 2A). This anterior part also has several symmetric connectives, as described in Bond-Buckup et al. (1991). The TG encloses five pairs of symmetrical limb-associated neuropils (Figs. 2A, 3C, 5C, 7E). From the caudal portion of the ganglion arises a branched nerve bundle that targets the pleomeres and the heart

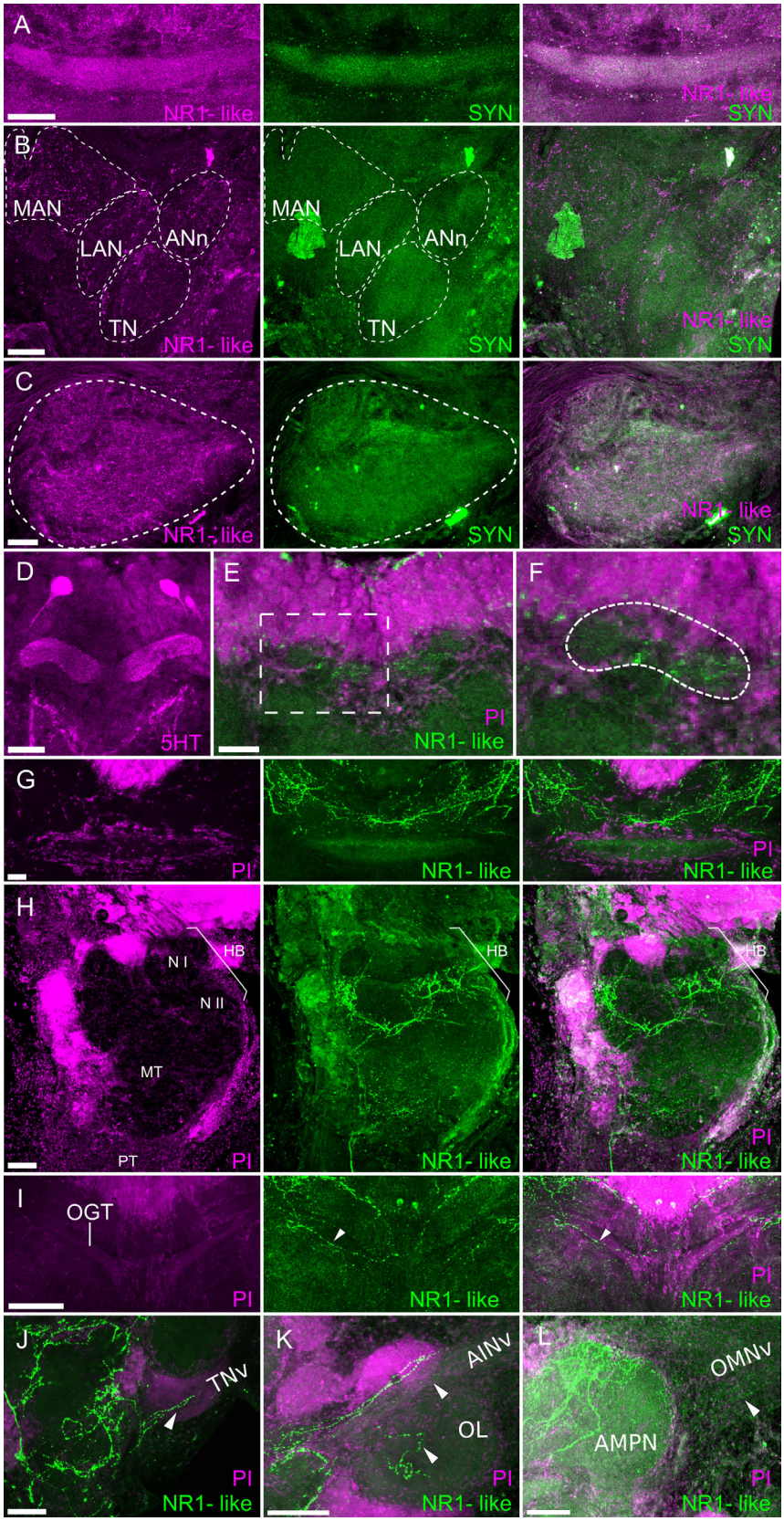
A
NR1- like
SYN
NR1- like
SYN
B
MAN
LAN
ANn
TN
NR1- like
MAN
LAN
ANn
TN
SYN
NR1- like
SYN
C
NR1- like
SYN
NR1- like
SYN
D
5HT
E
PI
NR1- like
F
G
PI
NR1- like
PI
NR1- like
H
N I
HB
N II
MT
PT
PI
HB
NR1- like
HB
PI
NR1- like
I
OGT
PI
NR1- like
PI
NR1- like
J
TNv
PI
NR1- like
K
AINv
OL
PI
NR1- like
L
OMNv
AMPN
PI
NR1- like

Figure 5

(Maynard, 1953; Bond-Buckup et al., 1991). In the center of the TG passes the descending sternal artery (Figs. 2A, 3C, 7E). The position of each ganglion in the crab body was schematized in a lateral view, excluding the chelae and the limbs (Fig. 2B).

Central brain: supraesophageal ganglion

The CBr (Fig. 3A,B,E) encloses the median protocerebrum, deutocerebrum, and tritocerebrum. The median protocerebrum can be subdivided into the anterior and posterior medial protocerebral neuropils (Fig. 4A). The protocerebral bridge is the V-shaped neuropil embedded in the anterior edge of the anterior medial protocerebral neuropil (Figs. 4A, 5D,E). Extending across the midline is the central body, which divides the anterior and posterior medial protocerebral neuropils (Fig. 4A). These two neuropils (protocerebral bridge and central body) have been the focus of several studies that collectively termed them the central complex (Utting et al., 2000; Homberg, 2008). The deutocerebrum includes the olfactory lobes, linked to the lateral protocerebrum via the olfactory globular tract, which crosses the CBr just dorsal to the central body and runs into the protocerebral tract (Sullivan and Beltz, 2001) (Fig. 4A). A central neuropil, the median antenna I neuropil is localized in a medial and posterior region of the deutocerebrum (Fig. 4A). On each side of the median antenna I neuropil, it is easy to observe the lateral antenna I neuropils and their connecting nerves: the antenna I nerve and the oculomotor nerve (Fig. 4A). The tritocerebrum contains two symmetrical pairs of neuropils: the antenna II and tegumentary neuropils. From the antenna II neuropil, the antenna II nerve emerges. The tegumentary neuropil is posterior to the lateral antenna I neuropil and connects centrifugally through the tegumentary nerves.

In the CBr, each neuropil area is associated with a group of somata, which are contained in clearly recognizable clusters. Based on their position and relation to neuropils, we recognized 12 clusters within the CBr, numbered 6 to 17, according to Sandeman's description (1–5 in the EG) (Sandeman et al., 1992). All clusters are symmetrical pairs, except for the 6th and 13th clusters (Figs. 3A, 4B). Each neuronal cluster will be described from the protocerebrum to tritocerebrum. The median protocerebrum includes a prominent medial cluster, the 6th, composed of heterogeneous somata lying anterior to the CBr and extending dorsally to ventrally in a V shape (Figs. 4B, 8A). Inferior to cluster 6 and adjacent to the midline, the 7th pair lies located in the ventral surface of the CBr (Fig. 4B). The 8th pair resides lateral to the posterior medial protocerebral neuropil (Fig. 4B). In *N. granulata*, we recognized an extra pair of clusters with small somata in the median protocerebrum, denoted cluster 18, following Sandman's numbering (Figs. 3A,B, arrowheads, and 4B, arrows). They are ventral and lateral to the 6th cluster, and they are situated in the most anterior part of the CBr. The described cell clusters in the deutocerebrum are groups of somata situated mainly on the ventral side (Fig. 3A, Ventral). Cluster 9 is located proximal to the anterior medial margin of the olfactory lobe and lateral and posterior to the posterior medial protocerebral neuropil (Fig. 4B). Cluster 10, with a more homogeneous cellular composition, is found attached to and posterior to the olfactory lobe (Fig. 4B). Cluster 11 is divided into two distinctive zones, one lateral homogeneous zone with small somata and another medial heterogeneous zone. This cluster is located between the olfactory lobe and the median antenna I neuropil on the dorsal side of the deutocerebrum (Fig. 4B). Together, cluster 12, a pair of heterogeneous somata that flank the cerebral artery, and cluster 13, a single medial cluster, surround the median antenna I neuropil on the ventral surface of the CBr (Fig. 4B). The following cell clusters were recognized in the tritocerebrum. The 14th pair lies laterally and dorsally on the external side of the antenna II neuropil (Fig. 4B). The small and laterally situated cluster 15 lies on the dorsal side of the CBr, over the posterior margin of the antenna II neuropil (Fig. 4B). Cluster 16 is located on

Figure 5. **A–C**: NR1-like and synapsin costaining. Left panels: NR1-like signal, Middle panels: synapsin signal (SYN). Right panels: Merge. A,B: Details of central brain neuropils. A: Central body. B: Median antenna I neuropil (MAN), Lateral antenna I neuropil (LAN), Tegumentary neuropil (TN), Antenna II neuropil (AnN). C: Detail of a thoracic ganglion neuropil. **D,E**: Central brain, detail of the protocerebral bridge. In D, Serotonin-like immunoreactivity (5HT). In E, NR1-like immunoreactivity and PI stain. Each image represents 12 μm of tissue thickness. **F**: Magnification of the PB from the area indicated by dotted square in E (dotted lines indicate the shape of the neuropil). **G–I**: Detail of NR1-like immunoreactivity. Left panel: PI stain; Middle panel: NR1-like immunoreactivity; Right panel: Merge. In G, central brain, detail of the central body. Image represents 30 μm of tissue thickness. In H, eyestalk ganglia, detail of the lateral protocerebrum indicating medulla terminalis (MT) and hemiellipsoid body (HB). NI, Neuropil 1; NII, Neuropil 2 of the hemielipsoid body. Image represents 200 μm of tissue thickness. PT: Protocerebral tract. In H, detail of the olfactory globular tract (OGT). **J–L**: Examples of NR1-like immunoreactivity in tracts, nerves and neuropils of the central brain. PI: Propidium iodide stain. In J, part of deutocerebral and tritocerebral neuropils are shown. TNv, tegumentary nerve. In K, detail of olfactory lobe (OL). AINv, Antenna I nerve. In L, Part of the anterior medial protocerebral neuropil (AMPN). OMNv, Oculomotor nerve. Arrowheads show positive immunoreactivity in the tracts and nerves indicated. Scale bars = 100 μm in A–C,G–I,J–L; 50 μm in D–F.

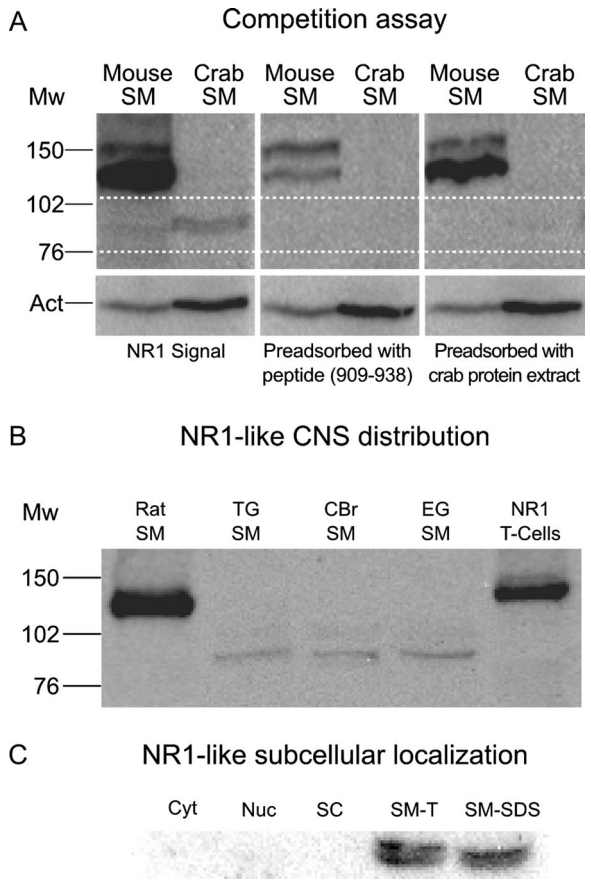

Figure 6. Identification of the NR1-like subunit by AB1516 Ab. **A**: Competition assay. Mouse and Crab SM extracts were run in SDS-PAGE, and the blots were incubated with one of the following: the primary antibody (NR1 Signal); the primary antibody preadsorbed with the synthetic peptide (aa 909–938); or the primary antibody preadsorbed with a crab protein extract (Crab SM with molecular weight ranging from ~76–102 kDa). Mw: Molecular weight. **B**: NR1-like CNS distribution. SM extracts from different crab ganglia (TG SM, SG SM, and EG SM), SM extracts from rat hippocampus (Rat SM), and total extracts from NR1-transfected HeLa cells (NR1 T-Cells), were run in SDS-PAGE and the blots were incubated with the anti-NR1 antibody. **C**: NR1-like subcellular localization. The following fractions were obtained by differential sedimentation: cytoplasmatic extract (Cyt), nuclear extract (Nuc), synaptosomal content (SC), and synaptosomal membranes treated with 1% Triton-X100 (SM-T) and with 1% sodium dodecyl sulfate (SMSDS); these were run in SDS-PAGE and the blots were incubated with anti-NR1 antibody.

the ventral surface of the CBr, between antenna II neuropil and median antenna I neuropil. Cluster 17 is a pair of ventrally and medially situated clusters with heterogeneous sizes. These clusters are located between the tracts that link the CBr with the TG, the circumesophageal connectives.

Characterization of the NR1-like subunit and its localization

We characterized *Neohelice* NMDA receptors using western blot assays and immunohistochemistry techniques. The NR1 subunit was studied because is an essential component of the NMDAR. The antibody used, AB1516 (Chemicon), is directed against the last 30 amino acids that correspond to the C-terminus of rat NR1 subunit (aa 909–938).

Western blot assays

To corroborate the NR1-like signal detected, the specificity of the AB1516 antibody was tested by preadsorbing the antibody (Fig. 6A). SDS-treated synaptosomal membranes (SM) from mouse and crab were run in SDS-PAGE, and the blots were subjected to three different conditions. The first blot was incubated with the primary antibody (NR1 Signal); in the second, the primary antibody was preadsorbed with the synthetic peptide that corresponded to the antigen sequence (peptide 909–938); and the third was incubated with the primary antibody preadsorbed with a crab protein extract obtained from crab SM, with molecular weights ranging from ~76–102 kDa.

Western blot analysis performed under the first conditions showed a strong band at ~124 kDa and another band at ~149 kDa in mouse SM (Fig. 6A). When the primary antibody was preadsorbed with the synthetic peptide, the intensity of the labeled ~124 kDa band decreased drastically relative to the NR1 signal. In addition, when the antibody was preadsorbed with crab protein extract, this band exhibited a lesser decrease. However, the ~149 kDa protein seemed to remain unchanged under the three tested conditions. Therefore, in mouse extract, the specific band that corresponded to the NR1 subunit had a molecular weight of ~124 kDa, similar to the expected molecular weight (~120 kDa; Fletcher et al., 2000). Two immunoreactive bands with molecular weights of ~88 and ~84 kDa were labeled in crab SM (Fig. 6A). In both preadsorbed conditions, the two labeled bands diminished notably. Therefore, two immunoreactive bands were specifically labeled in crab SM by employing this commercial antibody.

After testing the specificity, the localization of the NR1-like subunit in the CNS was studied using western blot assays. Synaptosomal membrane extracts from different tissues were used: TG, CBr, and EG (Fig. 6B). As a control, SM extracts from the rat hippocampus (Rat SM) and total extracts from NR1-transfected HeLa cells (NR1 T-Cells) were included in the assay. Immunoblotting with the anti-NR1 antibody yielded a ~116 kDa band in Rat SM and a ~124 kDa band in NR1-T cells (Fig. 6B). In the lines that corresponded to TG SM, CBr SM, and EG SM, it was

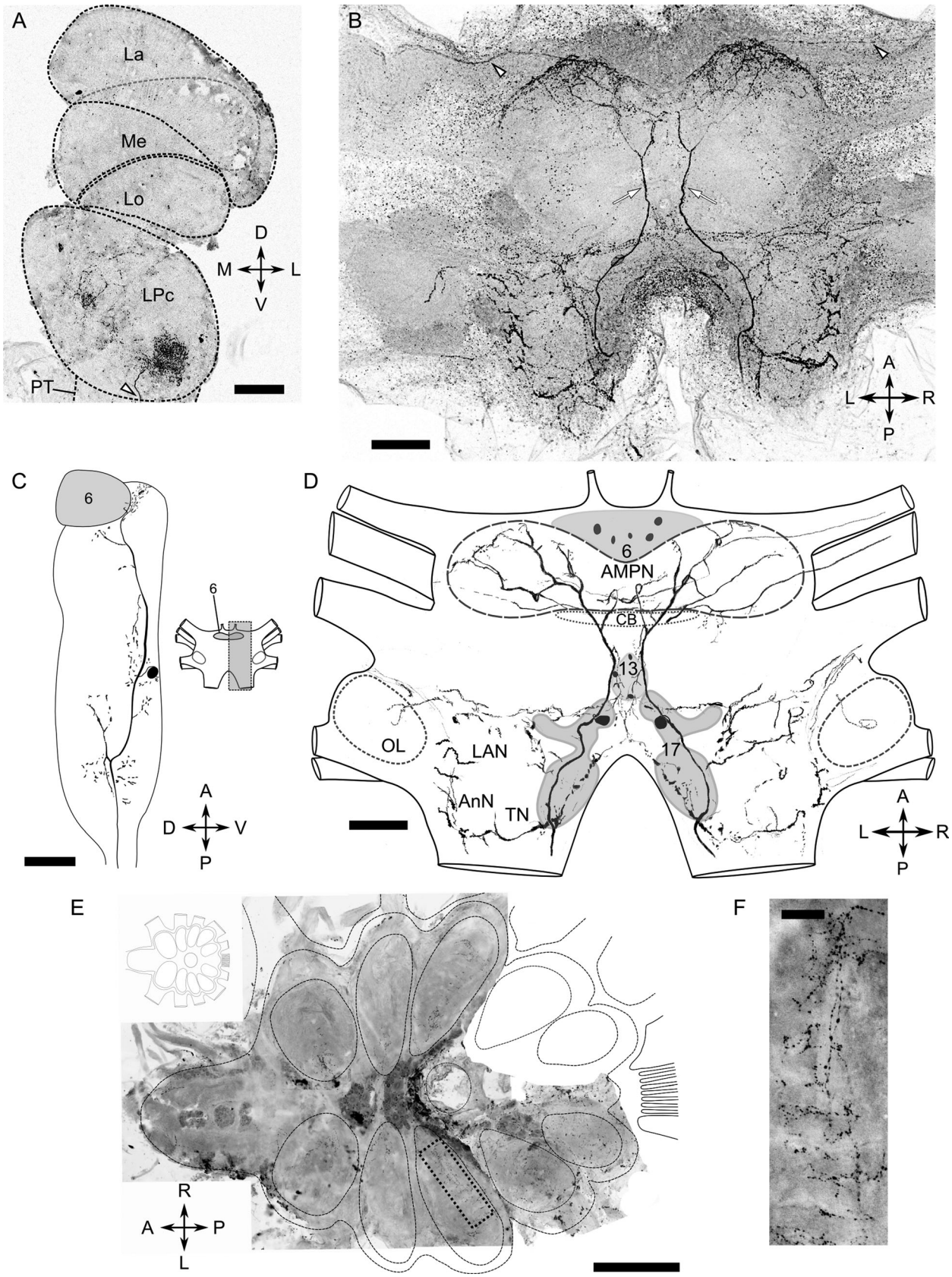
A
La
Me
Lo
LPc
PT
D
M
L
V
B
A
L
R
P
C
6
6
A
D
V
P
D
6
AMPN
CB
13
17
OL
LAN
AnN
TN
A
L
R
P
E
R
A
P
L
F

Figure 7

possible to observe an immunoreactive double band at ~86 kDa, which was identified as the unresolved ~84 and ~88 kDa bands, described in Figure 6A.

To evaluate the subcellular localization of the NR1-like subunit, the following fractions, obtained from TG by differential sedimentation, were used: cytoplasmatic extract (Cyt), nuclear extract (Nuc), synaptosomal content (SC), and synaptosomal membranes (SM). SM extract was treated with two detergents of increasing strength, first with 1% Triton X-100 (SM-T) and then with 1% SDS (SM-SDS). No bands were present in Cyt, Nuc, or SC (Fig. 6C). The expected immunoreactive bands were identified in the lines that corresponded to extracts enriched with SM (SM-T and SM-SDS) (Fig. 6C).

Immunohistochemistry techniques

The NR1-like protein localization was studied with immunohistochemistry techniques in the CNS of the crab *N. granulata*, using both whole-mount preparations and agarose-embedded sections. Using the AB1516 antibody, positive NR1-like immunoreactivity (NR1-ir) was found in each of the major ganglia, EG, CBr, and TG. Representative images obtained by confocal microscopy are displayed in Figure 7 (EG, A; CBr, B; TG, E). The neuropil that revealed most of the positive signal in the eyestalk ganglia was the lateral protocerebrum, showing arborizations in the ventral part of the medulla terminalis and the hemiellipsoid body (Figs. 5H, 7A). The staining displayed a complex pattern, which resembled dendrites and terminals. A conspicuous process was observed to run through the protocerebral tract, connecting the base of the lateral protocerebrum with the CBr (Figs. 5H, 7A,B, 8A).

Figure 8B shows a general view of the representative distribution of the NR1-like subunit in a whole-mount CBr. The signal in the CBr shows a bilateral symmetry. The main NR1-ir neurites run along the anterior–posterior axis (from PT to circumesophageal connectives, Fig. 7B; white arrowhead in 8A). Idealized schematic representations of the NR1-ir detected on the CBr were compiled (Fig. 7C,D). In a lateral view, the signal distribution was mainly ventral: 75% of the signal was located on the ventral side, and the remaining 25% was on the dorsal side (Fig. 7C). In a ventral view, the NR1-ir was detected in the three main divisions, median protocerebrum, deutocerebrum, and tritocerebrum, but displayed a particularly strong localization in the tritocerebrum (Figs. 5B, 7D, 8D). The NR1-ir was appreciable in neuropils and cell clusters. In neuropils, the staining represented processes and structures that resembled terminals and dendritic trees (Fig. 7B). The stained neuropils in the median protocerebrum were the anterior medial protocerebral neuropil (Figs. 5L, 7B,D, 8A), the protocerebral bridge (Figs. 5E,F, 8B), and the central body (Figs. 5A,G, 8A,C). Most of the neuropils presented in the deutocerebrum and tritocerebrum were labeled, namely, olfactory lobes, lateral antenna I neuropil, median antenna I neuropil, antenna II neuropil, and tegumentary neuropil (Figs. 5J,K, 7B,D, 8D). Several nerves of these neuropils, connectives, and some tracts were also stained: olfactory globular tract (Fig. 5I), which links the lateral protocerebrum with the olfactory lobes; oculomotor nerve (Fig. 5I) and antenna I nerve (Fig. 5K), which innervate the lateral antenna I neuropil; tegumentary nerve (Fig. 5J), which innervates the tegumentary neuropil and circumesophageal connectives (Figs. 7C,D, 8D, white arrowhead), which links the CBr with the TG. The NR1-ir inside the olfactory lobes was visible as a few strongly stained processes, which reached the lobe and spread between glomeruli. The NR1-like signal was present within the glomeruli in lower intensity (Figs. 5J,K, 7B).

In the neuronal clusters, the main somatic signal appeared in the tritocerebrum: two heavily labeled somata in the 17th cluster are symmetrically positioned (Fig. 7B,D) and have a considerable size, 38 μm ± 0.7 (mean maximum diameter ± SEM, $n = 18$) (Fig. 8D–F). From these somata, an NR1-ir primary neurite reaches a principal neurite (7 μm mean ± 0.39 SEM, $n = 11$) (Fig. 8E), with an anterior branch that runs toward the AMPN, where it arborizes, and one that runs posteriorly, toward the circumesophageal connective (Figs. 7B,D, 8E). These neurons have profuse arborizations in two main

Figure 7. NR1-like protein localization in the central nervous system of *Neohelice*. **A**: EG, general view of a representative image of NR1-ir detected on whole mount (z projection from 89 slices of 3 μm thickness). La, lamina; Me, medulla; Lo, lobula; LPc, lateral protocerebrum; PT, protocerebral tract. The cross indicates positions: D, dorsal; V, ventral; M, medial and L, lateral. **B**: SG, general view of a representative image of NR1-ir detected on whole mount (z projection, 100 slices of 3 μm thickness). Principal immunoreactive neurites are indicated by white arrows. The cross indicates positions: A, anterior; P, posterior; L, left and R, right. A,B: White arrowheads indicate immunoreactive processes that run through the PT, connecting the base of the LPc with the SG. **C**: Idealized scheme of NR1-ir detected in part of the SG, in a lateral view. The 6th cluster was highlighted (6, in gray). Inset: SG diagram. A gray box indicates the schematized NR1-ir area. The cross indicates positions: A, anterior; P, posterior; D, dorsal; V, ventral. **D**: Idealized scheme of NR1-ir detected in the SG, in a ventral view. OL, CB and AMPN (drawn in dotted lines). The cross indicates positions: A, anterior; P, posterior; L, left; R, right. **E**: TG NR1-ir. Image composed from 10× scans (z projection, 63 slices of 3 μm thickness) detected on a section. The cross indicates positions: A, anterior; P, posterior; L, left; R, right. **F**: Detail of the NR1-ir observed in a TG neuropil. Scale bars = 200 μm in A,B,D; 100 μm in C,F; 1,000 μm in E.

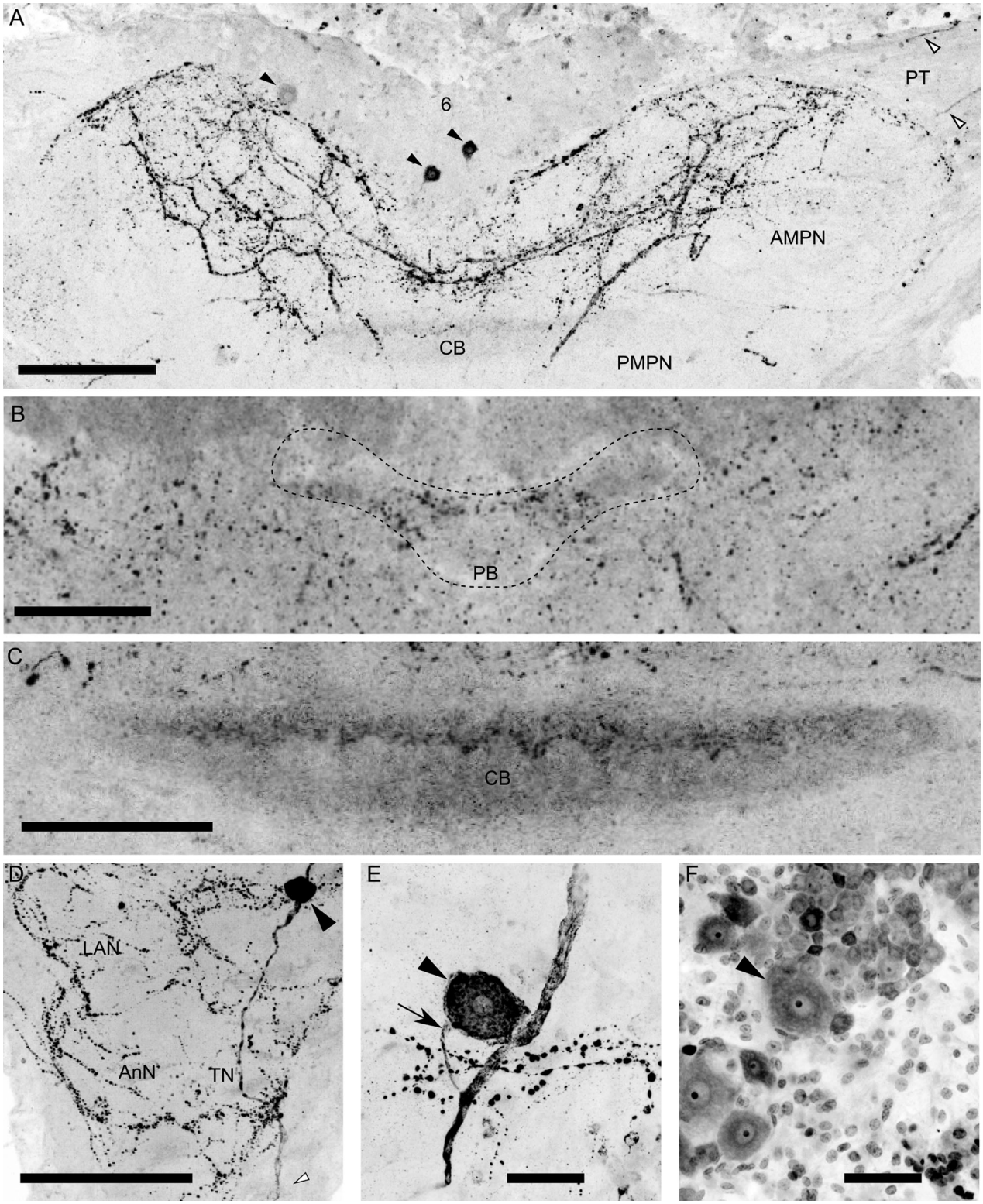

Figure 8. NR1-like protein localization in the SG. **A**: Detail of the anterior part of the SG NR1-ir, including the anterior (AMPN) and posterior (PMPN) medial protocerebral neuropils, the central body (CB), and the 6th cluster (6) (z projection, 20 slices of 3 μm thickness). White arrowheads indicate immunoreactive processes running through the PT, connecting the base of the LPc with the SG. **B**: Detail of the protocerebral bridge NR1-ir (CB, dotted line) (1 slice). **C**: Detail of the central body NR1-ir (CB) (z projection, 20 slices of 3 μm thickness). **D**: Detail of the tritocerebrum NR1-ir (z projection, 55 slices of 3 μm thickness). **E,F**: Detail of somas in the 17th cluster (black arrowhead) (z projection, 22 slices of 1 μm thickness). In E: NR1-ir soma, with their primary neurite (black arrow) and principal neurite. In F: Somas in the 17th cluster surrounding the NR1-ir soma, labeled with PI. Scale bars = 200 μm in A,D; 100 μm in B,C; 50 μm in E,F.

areas of the CBr, the anterior medial protocerebral neuropil and the posterior neuropils of the tritocerebrum. These two areas exhibit clear differences in the immunoreactivity of their processes (anterior medial protocerebral neuropil mean 2.92 ± 0.11 SEM vs. tritocerebrum mean 3.04 ± 0.15 SEM; $n = 6$; *t*-test: $P = 0.032$). In addition, smaller somata were identified in the 6th cluster of the median protocerebrum (Figs. 7D, 8A), and in the 13th cluster, medial and anterior to the 17th cluster (Fig. 7D).

A broad NR1-ir distribution in the thoracic ganglion was detected (Fig. 7E). From a reconstruction of the ganglion composed of projection images, it is possible to visualize central processes that arborize in each limb-associated neuropil (Figs. 5C, 7E,F). The NR1-ir appears in each neuropil as a group of main processes with regularly distributed, branching collaterals (Fig. 7F).

DISCUSSION

Given the central role of NMDARs in memory and plasticity, our research was focused on obtaining a detailed description of the distribution of NR1-like subunits at the neuropil level. Considering the fact that no neuroanatomical descriptions of the CNS of this crab as a whole currently exist, we first portrayed the different ganglia, maintaining the size relationships and locations in the animal. This map represents a new tool for future descriptive, molecular, and pharmacological approaches that employ this invertebrate model.

Neohelice granulata neuroanatomical description

Neohelice granulata presents a nervous system with a structural plan similar to that of other decapod crustaceans (Sandeman et al., 1992, 1993; Krieger et al., 2012). The optic ganglia and the lateral protocerebrum are situated in the eyestalks, located ~8 mm from the CBr. Inside the cephalothorax, a similar distance separates the CBr and the TG. Most neuropils and clusters described in the *Scylla serrata* CBr (Sandeman et al., 1992) are identifiable in *N. granulata* (see also: Frenkel et al., 2008; Fustiñana et al., 2010). The ganglion also exhibited many conspicuous connectives and tracts (i.e., antennal connectives and olfactory globular tract). Their approximated sizes are similar to the sizes observed in other decapods (Krieger et al., 2012). The number of publications that use *N. granulata* is increasing steadily, indicating that this crab species is a solid model for biochemical, physiological, and ecological research (reviewed in Spivak, 2010). For this reason, it is necessary to achieve a more complete neuroanatomical description of its nervous system.

Neohelice granulata NMDA-like receptors

In the *N. granulata* nervous system, it was possible to identify two immunoreactive bands for the NR1-like subunit (Fig. 6). The close proximity of the molecular weight of these bands suggests that they may represent post-translational modifications of one protein (Petralia et al., 1994; Rao and Craig, 1997), but we cannot rule out other possibilities, such as splicing variants (Hollmann et al., 1993). The competition assay with synthetic peptide suggests that some amino acid sequence homology might exist between mammalian and crustacean NMDARs.

The NR1-like bands were present in all of the major ganglia tested. The band intensities suggest an NR1-like homogenous distribution among ganglia (Fig. 6B). At a subcellular level, the NR1-like subunit is only detectable in synaptosomes, when Triton X-100 or SDS is used, which illustrates the synaptic membrane localization of this protein (Fig. 6C). As in western blots, immunohistochemistry revealed the presence of NR1-ir in all major ganglia (Fig. 7). The positive signal appears in neuronal clusters and neuropils, as well as in somata, processes, and terminals (Figs. 7, 8). In each ganglion, at low magnification, it is easy to recognize areas that exhibit a higher density of NR1-like subunits: the lateral protocerebrum in the EG, the anterior medial protocerebral neuropil and tritocerebral neuropils in the CBr, and the limb-associated neuropils in the TG. In decapods, some of these neuropils have been associated with sensory modalities; visual processing in protocerebral neuropils (lateral protocerebrum: Berón de Astrada and Tomsic, 2002; Sztarker et al., 2005; Medan et al., 2007; Krieger et al., 2010; median protocerebrum: Krieger et al., 2010; Berón de Astrada, pers. commun.); and mechanosensory processing in tritocerebral neuropils (Sandeman et al., 1993).

This wide distribution of NR1-like protein in *N. granulata* CNS may suggest potential areas of plasticity (Tsien et al., 1996; Xia et al., 2005; Ha et al., 2006). In the CBr, many of the stained processes and terminals seem to be components of two neurons. These neurons have prominent soma in the 17th cluster, which is connected to a thick principal neurite through a primary neurite (Fig. 7B) and arborizes anteriorly in the anterior medial protocerebral neuropil and posteriorly in the tritocerebral neuropils. The labeling in these two areas has distinctive NR1-ir particle sizes, smaller in the anterior medial protocerebral neuropil relative to the tritocerebral neuropils. Considering that NMDARs were reported in both pre- and postsynaptic sites (VanDongen, 2009) and that size and shape might be indicators of pre- and postsynaptic structures (Fischbach and Dittrich, 1989), the difference in the

NR1-ir sizes suggests a differential subcellular localization for each neuropil (anterior medial protocerebral neuropil and tritocerebral neuropils). This most likely represents a preferred directionality for the transmitted information.

In *Neohelice*, the two central complex neuropils, central body and protocerebral bridge, possess NR1-like immunoreactivity (Figs. 5A,E,F,G, 8B,C). In insects and crustaceans, these two central complex neuropils have similarities in location, connectivity and neurotransmitters (Utting et al., 2000; Harzsch, 2006; Homberg, 2008). In *Drosophila*, the presence of NMDARs in this complex is necessary for olfactory memory consolidation (Wu et al., 2007, Miyashita et al., 2012). Behavioral and pharmacological experiments from our laboratory indicate that NMDA-like receptors are involved in LTM in *N. granulata* (Pedreira et al., 2002; Troncoso and Maldonado, 2002; Pérez-Cuesta et al., 2007), and recent results indicate that a memory facilitating protocol implicates changes in the central body (Frenkel et al., 2010). Altogether, these data suggest that the strong staining observed in particular areas of the CNS of *N. granulata* might have a role in neuronal plasticity and memory storage and that the central complex neuropils are promising candidates for this purpose.

This work is the first description of NMDA-like receptor distribution in the CNS of a decapod. This thorough description of the nervous system will facilitate an understanding of how the system copes with memory processing and storage. Comprehending the role of these receptors in memory processes in *Neohelice*, and how they are modulated through experience, will be of particular importance in the future. Thus, studying how different areas contribute and interact during memory formation would allow comprehension of this process from a systemic point of view.

ACKNOWLEDGMENTS

We thank Angel Vidal for technical assistance and Dr. Julieta Sztarker and Dr. Martin Berón de Astrada for helpful discussions and revision of the article. We also thank Dr. Martin Federico Adrover for technical assistance with immunological techniques.

CONFLICTS OF INTEREST

There are no conflicts of interest.

ROLE OF AUTHORS

All authors had full access to all the data in the study and take responsibility for the integrity of the data and the accuracy of the data analysis. Study concept and design: MEP and RAMF. Acquisition of data: YH, MCT, and RAMF. Analysis and interpretation of data: YH, MCT, MEP, and RAMF. Drafting of the article: YH, MCT, MEP, and RAMF. Critical revision of the article for important intellectual content: YH, MCT, MEP, and RAMF. Statistical analysis: YH and RAMF. Obtained funding: MEP and RAMF. Administrative, technical, and material support: MEP and RAMF. Study supervision: MEP and RAMF.

LITERATURE CITED

Amano H, Maruyama IN. 2011. Aversive olfactory learning and associative long-term memory in Caenorhabditis elegans. Learn Mem 18:654–665.

Berón de Astrada M, Tomsic D. 2002. Physiology and morphology of visual movement detector neurons in a crab (Decapoda: Brachyura). J Comp Physiol A Neuroethol Sens Neural Behav Physiol 188:539–551.

Bicker G, Schäfer S, Ottersen OP, Storm-Mathisen J. 1988. Glutamate-like immunoreactivity in identified neuronal populations of insect nervous systems. J Neurosci 8: 2108–2122.

Bonasio R, Zhang G, Ye C, Mutti NS, Fang X, Qin N, Donahue G, Yang P, Li Q, Li C, Zhang P, Huang Z, Berger SL, Reinberg D, Wang J, Liebig J. 2010. Genomic comparison of the ants Camponotus floridanus and Harpegnathos saltator. Science 329:1068–1071.

Bond-Buckup G, Fontoura NF, Marroni NP, Kucharski LC. 1991. O'carangueijo–Manual para o ensino prático de zoologia. Ed. da Universidade, Univerdidade Federal do Rio Grande do Sul.

Brockie PJ, Mellem JE, Hills T, Madsen DM, Maricq AV. 2001. The C. elegans glutamate receptor subunit NMR-1 is required for slow NMDA-activated currents that regulate reversal frequency during locomotion. Neuron 31:617–630.

Browing K, Lukowiak K. 2008. Ketamine inhibits long-term, but not intermediate-term memory formation in Lymnaea stagnalis. Neuroscience 155:613–625.

Burgess MF, Derby CD. 1997. Two novel types of L-glutamate receptors with affinities for NMDA and L-cysteine in the olfactory organ of the Caribbean spiny lobster Panulirus argus. Brain Res 771:292–304.

Cain DP. 1997. LTP, NMDA, genes and learning. Curr Opin Neurobiol 2:235–242.

Carew TJ. 2000. Behavioral neurobiology. In: The cellular organization of natural behavior. Sunderland, MA: Sinauer.

Chiang AS, Liu YC, Chiu SL, Hu SH, Huang CY, Hsieh CH. 2001. Three-dimensional mapping of brain neuropils in the cockroach, Diploptera punctata. J Comp Neurol 440: 1–11.

Chiang AS, Pszczolkowski MA, Liu HP, Lin SC. 2002. Ionotropic glutamate receptors mediate juvenile hormone synthesis in the cockroach, Diploptera punctata. Insect Biochem Mol Biol 32:669–678.

Cull-Candy S, Brickley S, Farrant M. 2001. NMDA receptor subunits: diversity, development and disease. Curr Opin Neurobiol 11:327–335.

Dale N, Kandel ER. 1993. L-glutamate may be the fast excitatory transmitter of Aplysia sensory neurons. Proc Natl Acad Sci U S A 90:7163–7167.

Dingledine R, Borges K, Bowie D, Traynelis SF. 1999. The glutamate receptor ion channels. Pharmacol Rev 51:7–61.

Federman N, Fustiñana MS, Romano A. 2009. Histone acetylation is recruited in consolidation as a molecular feature of stronger memories. Learn Mem 16:600–606.

Federman N, Fustiñana MS, Romano A. 2012. Reconsolidation involves histone acetylation depending on the strength of the memory. Neuroscience 219:145–156.

Feinstein N, Parnas D, Parnas H, Dudel J, Parnas I. 1998. Functional and immunocytochemical identification of glutamate autoreceptors of an NMDA type in crayfish neuromuscular junction. J Neurophysiol 80:2893–2899.

Feld M, Dimant B, Delorenzi A, Coso O, Romano A. 2005. Phosphorylation of extra-nuclear ERK/MAPK is required for long-termmemory consolidation in the crab Chasmagnathus. Behav Brain Res 158:251–261.

Fischbach K-F, Dittrich APM. 1989. The optic lobe of Drosophila melanogaster. I. A Golgi analysis of wild-type structure. Cell Tissue Res 258:441–475.

Fletcher EL, Hack I, Brandstätter JH, Wässle H. 2000. Synaptic localization of NMDA receptor subunits in the rat retina. J Comp Neurol 420:98–112.

Frenkel L, Maldonado H, Delorenzi A. 2005. Memory strengthening by a real-life episode during reconsolidation: an outcome of water deprivation via brain angiotensin II. Eur J Neurosci 22:1757–1766.

Frenkel L, Dimant B, Portiansky EL, Maldonado H, Delorenzi A. 2008. Both heat shock and water deprivation trigger Hsp70 expression in the olfactory lobe of the crab Chasmagnathus granulatus. Neurosci Lett 443:251–256.

Frenkel L, Dimant B, Portiansky EL, Imboden H, Maldonado H, Delorenzi A. 2010. Neuroanatomical distribution of angiotensin-II-like neuropeptide within the central nervous system of the crab Chasmagnathus; physiological changes triggered by water deprivation. Cell Tissue Res 341: 181–195.

Frenkel L, Dimant B, Suárez LD, Portiansky EL, Delorenzi A. 2012. Food odor, visual danger stimulus, and retrieval of an aversive memory trigger heat shock protein HSP70 expression in the olfactory lobe of the crab Chasmagnathus granulatus. Neuroscience 201:239–251.

Freudenthal R, Locatelli F, Hermitte G, Maldonado H, Delorenzi A, Romano A. 1998. NFκB-like DNA binding activity is enhanced after spaced training that induces long-term memory in the crab Chasmagnathus. Neurosci Lett 242:143–146.

Furukawa F, Grouaux E. 2003. Mechanisms of activation, inhibition and specificity: crystal structures of the NMDA receptor NR1 ligand-binding core. EMBO J 22:2873–2885.

Fustiñana MS, Ariel P, Federman N, Freudenthal R, Romano A. 2010. Characterization of the beta amyloid precursor protein-like gene in the central nervous system of the crab Chasmagnathus. Expression during memory consolidation. BMC Neurosci 11:109.

Gallus L, Ferrando S, Gambardella C, Diaspro A, Bianchini P, Faimali M, Ramoino P, Tagliafierro G. 2010. NMDA R1 receptor distribution in the cyprid of Balanus amphitrite (=Amphibalanus amphitrite) (Cirripedia, Crustacea). Neurosci Lett 485:183–188.

Grey KB, Moss BL, Burrell BD. 2009. Molecular identification and expression of the NMDA receptor NR1 subunit in the leech. Invert Neurosci 9:11–20.

Gutiérrez H, Gutiérrez R, Silva-Gandarias R, Estrada J, Miranda MI, Bermúdez-Rattoni F. 1999. Differential effects of 192IgG-saporin and NMDA-induced lesions into the basal forebrain on cholinergic activity and taste aversion memory formation. Brain Res 834:136–141.

Ha TJ, Kohn AB, Bobkova YV, Moroz LL. 2006. Molecular characterization of NMDA-like receptors in Aplysia and Lymnaea: relevance to memory mechanisms. Biol Bull 210: 255–270.

Harzsch S. 2006. Neurophylogeny: architecture of the nervous system and a fresh view on arthropod phyologeny. Integr Comp Biol 46:162–194.

Harzsch S, Hansson BS. 2008. Brain architecture in the terrestrial hermit crab Coenobita clypeatus (Anomura, Coenobitidae), a crustacean with a good aerial sense of smell. BMC Neurosci 9:58.

Harzsch S, Miller J, Benton J, Beltz B. 1999. From embryo to adult: persistent neurogenesis and apoptotic cell death shape the lobster deutocerebrum. J Neurosci 19: 3472–3485.

Hepp Y, Pérez-Cuesta LM, Maldonado H, Pedreira ME. 2010. Extinction memory in the crab Chasmagnathus: recovery protocols and effects of multi-trial extinction training. Anim Cogn 13:391–403.

Hollmann M. 1999. Structure of ionotropic glutamate receptors. In: Jonas P, Monyer H, editors. Ionotropic glutamate receptors in the CNS. Berlin: Springer. p 1–98.

Hollmann M, Boulter J, Maron C, Beasley L, Sullivan J, Pecht G, Heinemann S. 1993. Zinc potentiates agonist-induced currents at certain splice variants of the NMDA receptor. Neuron 10:943–954.

Homberg U. 2008. Evolution of the central complex in the arthropod brain with respect to the visual system. Arthropod Struct Dev 37:347–362.

Kano T, Brockie PJ, Sassa T, Fujimoto H, Kawahara Y, Iino Y, Mellem JE, Madsen DM, Hosono R, Maricq AV. 2008. Memory in Caenorhabditis elegans is mediated by NMDA-type ionotropic glutamate receptors. Curr Biol 18:1010–1015.

Klagges BR, Heimbeck G, Godenschwege TA, Hofbauer A, Pflugfelder GO, Reifegerste R, Reisch D, Schaupp M, Buchner S, Buchner E. 1996. Invertebrate synapsins: a single gene codes for several isoforms in Drosophila. J Neurosci 16:3154–3165.

Krieger J, Sandeman RE, Sandeman DC, Hansson BS, Harzsch S. 2010. Brain architecture of the largest living land arthropod, the Giant Robber Crab Birgus latro (Crustacea, Anomura, Coenobitidae): evidence for a prominent central olfactory pathway? Front Zool 7:25.

Krieger J, Sombke A, Seefluth F, Kenning M, Hansson BS, Harzsch S. 2012. Comparative brain architecture of the European shore crab Carcinus maenas (Brachyura) and the common hermit crab Pagurus bernhardus (Anomura) with notes on other marine hermit crabs. Cell Tissue Res 348:47–69.

Lin XY, Glanzman DL. 1994. Hebbian induction of long-term potentiation of Aplysia sensorimotor synapses: partial requirement for activation of an NMDA-related receptor. Proc Biol Sci 255:215–221.

Lin XY, Glanzman DL. 1997. Effect of interstimulus interval on pairing-induced LTP of Aplysia sensorimotor synapses in cell culture. J Neurophysiol 77:667–674.

Locatelli F, Romano A. 2005. Differential activity profile of cAMP-dependent protein kinase isoforms during long-term memory consolidation in the crab Chasmagnathus. Neurobiol Learn Mem 83:232–242.

Maldonado H. 2002. Crustaceans as models to investigate memory illustrated by extensive behavioral and physiological studies in Chasmagnathus. In: Wiese E, editor. The crustacean nervous system. Berlin: Springer. p 314–327.

Mayer ML, Benveniste M, Patneau DK. 1994. NMDA receptor agonists and competitive antagonists. In: Collingridge GL, Watkins JC, editors. The NMDA receptor, 2nd ed. New York: Oxford University Press. p 132–146.

Maynard DR. 1953. Activity in a crustacean ganglion. I. Cardioinhibition and acceleration in Panulirus argus. Biol Bull 104:156–170.

McBain CJ, Mayer ML. 1994. N-methyl-D-aspartic acid receptor structure and function. Physiol Rev 74:723–760.

McLaughlin PA. 1983. Internal anatomy. In: Bliss DE, editor, The biology of Crustacea, vol. 5. New York: Academic Press. p 41.

Medan V, Oliva D, Tomsic D. 2007. Characterization of lobula giant neurons responsive to visual stimuli that elicit escape behaviors in the crab Chasmagnathus. J Neurophysiol 98: 2414–2428.

Merlo E, Romano A. 2007. Long-term memory consolidation depends on proteasome activity in the crab Chasmagnathus. Neuroscience 147:46–52.

Merlo E, Romano A. 2008. Memory extinction entails the inhibition of the transcription factor NF-kappaB. PLoS One 3: e3687.

Miserendino MJ, Sananes CB, Melia KR, Davis M. 1990. Blocking of acquisition but not expression on conditioned fear-potentiated startle by NMDA antagonists in the amygdala. Nature 345:716–718.

Miyashita T, Oda Y, Horiuchi J, Yin JC, Morimoto T, Saitoe M. 2012. Mg(2+) block of Drosophila NMDA receptors is required for long-term memory formation and CREB-dependent gene expression. Neuron 74:887–898.

Moroz LL, Györi J, Salánki J. 1993. NMDA-like receptors in the CNS of molluscs. Neuroreport 4:201–204.

Morris RG, Anderson E, Lynch GS, Baudry M. 1986. Selective impairment of learning and blockade of long-term potentiation by an N-methyl-D-aspartate receptor antagonist, AP5. Nature 319:774–776.

Müβig L Richlitzki A, Rössler R, Eisenhardt D, Menzel R, Leboulle G. 2010. Acute disruption of the NMDA receptor subunit NR1 in the honeybee brain selectively impairs memory formation. J Neurosci 30:7817–7825.

Nässel DR, Elofsson R. 1987. Comparative anatomy of the crustacean brain. In: Gupta AP, editor. Arthropod brain. New York: John Wiley & Sons. p 111–135.

Papadakis M, Hawkins LM, Stephenson FA. 2004. Appropriate NR1-NR1 disulfide-linked homodimer formation is requisite for efficient expression of functional, cell surface N-methyl-D-aspartate NR1/NR2 receptors. J Biol Chem 279: 14703–14712.

Parnas H, Parnas I, Ravin R, Yudelevitch B. 1994. Glutamate and N-methyl-D-aspartate affect release from crayfish axon terminals in a voltage-dependent manner. Proc Natl Acad Sci U S A 91:11586–11590.

Parnas I, Dudel J, Parnas H, Ravin R. 1996. Glutamate depresses release by activating non-conventional glutamate receptors at crayfish nerve terminals. Eur J Neurosci 8:116–126.

Pedreira ME, Maldonado H. 2003. Protein synthesis subserves reconsolidation or extinction depending on reminder duration. Neuron 38:863–869.

Pedreira ME, Pérez-Cuesta LM, Maldonado H. 2002. Reactivation and reconsolidation of long-term memory in the crab Chasmagnathus: protein synthesis requirement and mediation by NMDA-type glutamatergic receptors. J Neurosci 32: 8305–8311.

Pérez-Cuesta LM, Maldonado H. 2009. Memory reconsolidation and extinction in the crab: mutual exclusion or coexistence? Learn Mem 16:714–721.

Pérez-Cuesta LM, Hepp Y, Pedreira ME, Maldonado H. 2007. Extinction is not developed along with CS presentation but within a few seconds after CS-offset. Learn Mem 14: 101–108.

Petralia RS, Wang YX, Wenthold RJ. 1994. The NMDA receptor subunits NR2A and NR2B show histological and ultrastructural localization patterns similar to those of NR1. J Neurosci 14:6102–6020.

Pfeiffer-Linn C, Glantz RM. 1991. An arthropod NMDA receptor. Synapse 9:35–42.

Rao A, Craig AM. 1997. Activity regulates the synaptic localization of the NMDA receptor in hippocampal neurons. Neuron 19:801–812.

Richter S, Loesel R, Purschke G, Schmidt-Rhaesa A, Scholtz G, Stach T, Vogt L, Wanninger A, Brenneis G, Döring C, Faller S, Fritsch M, Grobe P, Heuer CM, Kaul S, Møller OS, Müller CH, Rieger V, Rothe BH, Stegner ME, Harzsch S. 2010. Invertebrate neurophylogeny: suggested terms and definitions for a neuroanatomical glossary. Front Zool 7:29.

Rickard NS, Poot AC, Gibbs ME, Ng KT. 1994. Both non-NMDA and NMDA glutamate receptors are necessary for memory consolidation in the day-old chick. Behav Neural Biol 62:33–40.

Rieger AM, Hall BE, Luong le T, Schang LM, Barreda DR. 2010. Conventional apoptosis assays using propidium iodide generate a significant number of false positives that prevent accurate assessment of cell death. J Immunol Methods. 358:81–92.

Roberts AC, Glanzman DL. 2003. Learning in Aplysia: looking at synaptic plasticity from both sides. Trends Neurosci 26: 662–670.

Romano A, Locatelli F, Freudenthal R, Merlo E, Feld M, Ariel P, Lemos D, Federman N, Fustiñana MS. 2006. Lessons from a crab: molecular mechanisms in different memory phases of Chasmagnathus. Biol Bull 210:280–288.

Rosenegger D, Lukowiak K. 2010. The participation of NMDA receptors, PKC, and MAPK in the formation of memory following operant conditioning in Lymnaea. Mol Brain 3: 24.

Sandeman DC. 1982. Organization of the central nervous system. In: Atwo HL, Sandeman DC, editors. The biology of the crustacean, vol. 3. Neurobiology of structure and function. New York: Academic Press. p 1–61.

Sandeman DC, Sandeman RE, Derby C, Schmidt M. 1992. Morphology of the brain of crayfish, crabs, and spiny lobsters: a common nomenclature for homologous structures. Biol Bull 183:304–326.

Sandeman DC, Schoutz G, Sandeman RE. 1993. Brain evolution in decapod crustacea. J Exp Zool 265:112–133.

Schramm M, Dudel J. 1997. Metabotropic glutamate autoreceptors on nerve terminals of crayfish muscle depress or facilitate release. Neurosci Lett 234:31–34.

Shibata K, Tarui A, Todoroki N, Kawamoto S, Takahashi S, Kera Y, Yamada R. 2001. Occurrence of N-methyl-L-aspartate in bivalves and its distribution compared with that of N-methyl-D-aspartate and D,L-aspartate. Comp Biochem Physiol B Biochem Mol Biol 130:493–500.

Si A, Helliwell P, Maleszka R. 2004. Effects of NMDA receptor antagonists on olfactory learning and memory in the honeybee (Apis mellifera). Pharmacol Biochem Behav 77: 191–197.

Sinakevitch I, Farris SM, Strausfeld NJ. 2001. Taurine-, aspartate- and glutamate-like immunoreactivity identifies chemically distinct subdivisions of Kenyon cells in the cockroach mushroom body. J Comp Neurol 439:352–367.

Spivak ED. 2010. The crab Neohelice (=Chasmagnathus) granulata: an emergent animal model from emergent countries. Helgoland Marine Res 64:149–154.

Strausfeld NJ. 2002. Organization of the honey bee mushroom body: representation of the calyx within the vertical and gamma lobes. J Comp Neurol 450:4–33.

Sullivan JM, Beltz BS. 2001. Neural pathways connecting the deutocerebrum and lateral protocerebrum in the brains of decapod crustaceans. J Comp Neurol 441:9–22.